How space-filling are eddies? An analysis of energy- and flux-carrying coherent structures in turbulent channel flow

By A. Elnahhas

1. Motivation and objectives

The coherent structure approach to turbulence postulates that a turbulent flow, as opposed to being an amorphous fluctuating soup, is composed of a collection of distinct structures, called eddies, which advect, deform, and interact with one another (Robinson 1991). However, these turbulent eddies are difficult to define accurately. Nevertheless, several attempts at constructing coherent structure–based models of turbulence start from candidate building blocks inspired by observations of the flow. In homogeneous isotropic turbulence, candidate building-block eddies include the stretched vortex model (Lundgren 1982). In the case of wall-bounded turbulence, the most famous conceptual coherent structure model is the attached-eddy model, where self-similar hierarchies scaling with distance from the wall are superposed to reconstruct the fluctuating statistics (Townsend 1976; Marusic & Monty 2019). While the conceptual attached-eddy model makes no statements about the shapes of these building-block eddies, the inclined Λ-vortex has been the go-to candidate following the work of Perry & Chong (1982). In this work, we choose a qualitative description for coherent structures, namely that turbulent eddies are regions of space which are coherent in some property at some time instant, and maintain this coherence over some appreciable time (Adrian 2007).

This qualitative description of an eddy is important for two reasons. Firstly, we do not limit ourselves to asking questions about eddies formed from a single flow quantity, such as vorticity. Secondly, we do not restrict ourselves to specific shapes, such as Λ-vortices. This is important, as once a choice is made about either a flow quantity to threshold or a specific shape to look for, several questions immediately arise. Are the identified regions of the flow given a specific property representative of the entirety of the flow; i.e., would picking a different flow quantity to threshold highlight the same regions of activity, or different ones? Does this change with scale? What lies in between the identified regions? The goal of this work is to probe the answers to these questions from a static viewpoint in the absence of dynamics.

To maintain as minimal a bias as possible, we define both energy- and flux-carrying eddies, based on the the Reynolds-stress budget equations. We then decompose the flow field into the maximum number of regions of intense activity for each eddy type using a percolation analysis, as was done by Del Álamo & Jiménez (2006), Lozano-Durán *et al.* (2012), Lozano-Durán *et al.* (2014), Dong *et al.* (2020), Bae & Lee (2021), and Elnahhas *et al.* (2022, 2024). This approach was previously shown to seamlessly extract both wall-attached and -detached structures. For the identified regions of all eddy types, we compute how much space, on average, they occupy of the full domain, how much space they occupy in the aggregate, and how much space is occupied by regions of intersection between any two types of eddies. Given these results, we propose a condition for

identifying "at-a-distance" interactions between two eddies, which is essential for further spatiotemporal analyses aimed at extracting the key dynamical processes of wall-bounded turbulence in both physical and scale space (Elnahhas *et al.* 2024).

The report is organized as follows. Section 2 discusses the direct numerical simulation (DNS) channel flow data used for the analysis; a summary of the algorithm used to extract the various eddy types; and all eddy type definitions, including energy- and flux-carrying eddies, motivated using the normal Reynolds-stress budget equations. Section 3 presents the relative volumetric intersection matrix for all analyzed eddy types, for both all types of structures and only those that are attached. Furthermore, a plausible condition for identifying "at-a-distance" interactions is also proposed in this section. Finally, section 4 presents the conclusions and future work.

2. Dataset and approach

2.1. *DNS dataset*

The flow analyzed is a DNS of a channel at a friction Reynolds number, $Re_\tau = 550$, where $Re_\tau = u_\tau \delta/\nu$, with u_τ being the friction velocity, δ being the channel half-height, and ν being the kinematic viscosity. The flow velocity is denoted by u, v, and w, corresponding to the velocity in the streamwise, x, wall-normal, y, and spanwise, z, directions, respectively. The velocity components can be decomposed into a mean, U, and fluctuating components, u', v', and w'. We interchangeably use index notation to denote these velocity and coordinate components as u_i and x_i, respectively, for $i = \{1, 2, 3\}$. The domain of the channel has a size of $\{2\pi \times 2 \times \pi\}\delta$ with a resolution in inner wall units of $\{\Delta_x^+, \Delta_{y,\min}^+, \Delta_{y,\max}^+, \Delta_z^+\} = \{6.75, 0.34, 8.60, 6.75\}$. After reaching a statistically stationary state, 284 individual flow fields spaced $\Delta t^+ \approx 35$ apart are used to extract structures for further analysis. The total time from which statistics are extracted is therefore approximately $18\tau_{eddy}$, where $\tau_{eddy} = \delta/u_\tau$ is the large-scale eddy turnover time.

2.2. *Structure identification algorithm*

The clustering algorithm is based on identifying connected regions of space which all clear, in an absolute amplitude sense, a (wall-normally varying) threshold (Lozano-Durán *et al.* 2012). This is generically defined for an arbitrary flow property, f_p, and threshold, $f_t(y)$, as

$$\Omega_{f_p}(t) = \bigcup_{i=1}^{N} \omega_{f_p}^i(t) = \{(x, y, z) : |f_p(x, y, z, t)| > H_{f_p} f_t(y)\}, \tag{2.1}$$

where $\omega_{f_p}^i(t)$ denote the individual regions associated with individual eddies at some time t, $\Omega_{f_p}(t)$ denotes the union of regions of N eddies at some time t, and H_{f_p} is the f_p-dependent hyperbolic hole size. The physical volumes occupied by $\omega_{f_p}^i(t)$ and $\Omega_{f_p}(t)$, are denoted by $V(\omega_{f_p}^i(t))$ and $V(\Omega_{f_p}(t))$, respectively. For the example of momentum-flux-carrying structures, namely three-dimensional quadrants, $\mathcal{Q}$, $f_p = u'v'$, and $f_t(y) = u_{rms}(y)v_{rms}(y)$. In this study, H_{f_p} is varied such that the temporally averaged number of structures of each individual eddy type defined below is maximized.

2.3. *Defining energy- and flux-carrying eddies*

Regions of space can either carry a quantity or carry a flux of said quantity from one region to another, or across scales. This interpretation is motivated by the two sides of a

generic advection-diffusion equation integrated over some spatiotemporally varying volume (including filtering in the case of scale analysis). In essence, some quantity, a primary example being energy, $\mathcal{E}$, is carried within the bulk of some identified region, $\omega_{\mathcal{E}}(t)$, with fluxes, $\mathcal{F}_{\mathcal{E}}$, across the spatiotemporally varying boundary, $\partial\omega_{\mathcal{E}}(t)$, adjusting the value of energy within $\omega_{\mathcal{E}}(t)$. Of course, another region of space, $\omega_{\mathcal{F}_{\mathcal{E}}}(t)$, can be associated with intense energy flux, and it is the volumetric intersections between them, $V(\omega_{\mathcal{E}} \cap \omega_{\mathcal{F}_{\mathcal{E}}})$, which we desire to explore, as they imply an intense flux across the boundaries of the regions of that thresholded quantity, heavily modifying it.

In this work, we limit ourselves to identifying structures based on the quantities which appear on the two sides of the averaged, normal Reynolds-stress equations (Mansour *et al.* 1988), along with the fluxes of momentum in the fluctuating momentum equation. This ensures that while we are are studying the spatial properties of fluctuating turbulent eddies, the average over all eddies contributes in a non-trivial way to the mean balance of the flow energetics. The averaged Reynolds-stress budget equations, written in source, sink, and flux form, are

$$\frac{\overline{D}}{Dt}\overline{u_i' u_j'} = \mathcal{P}_{ij} - \epsilon_{ij} + \frac{\partial}{\partial x_k}(\mathcal{F}_{T,ijk} + \mathcal{F}_{D,ijk} + \mathcal{F}_{p,ijk}) + \mathcal{PS}_{ij}, \tag{2.2}$$

where

$$\mathcal{P}_{ij} = -\left[\overline{u_i' u_k'}\frac{\partial U_j}{\partial x_k} + \overline{u_j' u_k'}\frac{\partial U_i}{\partial x_k}\right] \rightarrow \text{production rate}, \tag{2.3}$$

$$\epsilon_{ij} = 2\nu\overline{\frac{\partial u_i'}{\partial x_k}\frac{\partial u_j'}{\partial x_k}} \rightarrow \text{dissipation rate}, \tag{2.4}$$

$$\mathcal{F}_{T,ijk} = -\overline{u_i' u_j' u_k'} \rightarrow \text{turbulent flux of } \overline{u_i' u_j'}, \tag{2.5}$$

$$\mathcal{F}_{D,ijk} = -\nu\frac{\partial \overline{u_i' u_j'}}{\partial x_k} \rightarrow \text{diffusive flux of } \overline{u_i' u_j'}, \tag{2.6}$$

$$\mathcal{F}_{p,ijk} = -\frac{1}{\rho}\left[\overline{p' u_i'}\delta_{jk} + \overline{p' u_j'}\delta_{ik}\right] \rightarrow \text{pressure diffusive flux of } \overline{u_i' u_j'}, \tag{2.7}$$

$$\mathcal{PS}_{ij} = \frac{2}{\rho}\overline{p' s_{ij}'} \rightarrow \text{pressure strain correlation exchange of } \overline{u_i' u_j'}, \tag{2.8}$$

where p' is the fluctuating pressure field, δ_{ij} is the Kronecker delta tensor, and s_{ij}' is the fluctuating rate-of-strain tensor. We can see that on the left-hand side of Eq. 2.2, an energetic quantity is being advected, and on the right-hand side, local sources and sinks, such as production and dissipation, act upon it, while various kinds of flux redistribute the energetic quantity in space and among components. It is this equation which we interpret instantaneously and non-locally to define our structures. We further limit ourselves to distinguishing only between streamwise and cross-stream terms, henceforth labeled with superscript S and CS, respectively. The exact local eddy definitions along with their respective hyperbolic hole strengths are defined in Table 1. For each of those eddy types, the wall-normal dependent threshold profile is the root-mean-squared profile of that particular quantity.

Eddy Label	f_p	H_{f_p}	$\overline{V}(\Omega_{f_p})$ (%)	$\overline{V}(\Omega_{f_p}^{\mathcal{A}})$ (%)
$\mathcal{Q}$	$u'v'$	1.15	17.89	14.70
$\mathcal{S}$	$\sqrt{u'^2+w'^2}$	1.95	7.73	6.33
$\mathcal{R}$	$\sqrt{v'^2+w'^2}$	1.65	7.42	5.57
p	p'	1.35	14.61	11.85
$\mathcal{P}$	$-u'v'\frac{\partial U}{\partial y}$	1.15	15.55	12.44
ϵ	$2\nu s'_{ij}s'_{ij}$	2.55	5.04	2.48
$\mathcal{D}$	$\mathcal{D}$	0.01525	7.05	4.47
$\mathcal{F}^S_{\text{Turb.}}$	u'^2v'	0.75	13.49	11.02
$\mathcal{F}^{CS}_{\text{Turb.}}$	$(v'^2+w'^2)v'$	1.30	7.83	4.82
$\mathcal{F}^S_{\text{Diff.}}$	$\nu\frac{\partial u'^2}{\partial y}$	1.60	7.66	3.79
$\mathcal{F}^{CS}_{\text{Diff.}}$	$\nu\frac{\partial (v'^2+w'^2)}{\partial y}$	1.45	9.43	5.36
$\mathcal{F}_{\text{Press.}}$	$p'v'$	1.10	12.51	9.42
$\mathcal{PS}^S$	$p's'_{11}$	1.00	12.85	7.63
$\mathcal{PS}^{CS}$	$p'(s'_{22}+s'_{33})$	1.00	12.54	7.99

TABLE 1. The first three columns indicate the eddy type, along with its instantaneous local definition and the hyperbolic hole size, H_{f_p}, for that particular eddy type used to maximize the average number of objects in a single snapshot of the flow using a percolation analysis. The fourth column indicates the average percentage, where $\overline{(.)}$ denotes the average over time, of the volume of the domain occupied by the different eddy types. The last column indicates this average volume occupancy contributed by eddies that are attached to the wall.

3. The space-filling properties of energy- and flux-carrying eddies

3.1. *Volumetric occupancy*

We first examine the average total volume occupied by each individual eddy type, $\overline{V}(\Omega_{f_p})$. Table 1 shows that the total volume occupied by any individual eddy type does not exceed 18% of the volume of the domain, with wall-normal momentum flux eddies, $\mathcal{Q}$, occupying the most volume. The smallest portion of the domain is occupied by intense isotropic dissipation structures at around 5%. This is in line with our expectation that $\mathcal{Q}$ structures are representative of the large scales of the flow while ϵ structures represent the small scales, which are more intermittent and hence contain most of the contribution to their averages in localized, intense pockets of space (Frisch 1995).

Figure 1 depicts a representative joint probability distribution function (PDF) of the minimal, y^+_{min}, and maximal, y^+_{max}, wall-normal extents of the identified streaky structures, $\mathcal{S}$. The main feature of this PDF, which is consistent with the work of Lozano-Durán *et al.* (2012), is the existence of two distinct families of structures. The first consists of wall-detached structures represented by the diagonal contours, whose width, $y^+_{max}-y^+_{min}$, does not vary substantially with height, $(y^+_{max}+y^+_{min})/2$. The second consists of wall-attached structures anchored below $y^+\approx 20$ and extending far into the center of the channel, with some excursions above the channel half-height. These wall-attached structures are much larger and contribute most of the volume of the identified structures of any particular type, even though their counts are usually around 30% of the total identified structures. The only exception are the vortex clusters, defined using the discriminant of the velocity gradient tensor, $\mathcal{D}$, where only 15% of their identified eddies are attached. The two families of structures are found for all the different eddy types

considered in this study, with similar PDFs to the one presented in Figure 1. Therefore, we can decompose Ω_{f_p} into two sets of eddies as follows

$$\Omega_{f_p}(t) = \Omega^{\mathcal{A}}_{f_p}(t) \cup (\Omega_{f_p}(t) \backslash \Omega^{\mathcal{A}}_{f_p}(t)), \tag{3.1}$$

where $\Omega^{\mathcal{A}}_{f_p}(t)$ denotes the union of attached eddies defined as

$$\Omega^{\mathcal{A}}_{f_p}(t) = \bigcup_{i=1}^{N_{\mathcal{A}}} \omega^i_{f_p}(t) = \{(x,y,z) : |f_p(x,y,z,t)| > H_{f_p} f_t(y) \quad \& \quad \min\left(\frac{y u_\tau}{\nu}\right) < 20\}, \tag{3.2}$$

with the number of attached eddies, $N_{\mathcal{A}} \leq N$.

By isolating the total volume occupied by only the attached clusters of each eddy type, we find the total volume occupancy for each eddy type, presented in the last column of Table 1. For quantities that depend on the streamwise velocity fluctuations or are proportional to them, i.e., $\mathcal{Q}$, $\mathcal{S}$, p, $\mathcal{P}$, and $\mathcal{F}^S_{\text{Turb.}}$, the attached clusters contribute between 80% and 82% of the volume of all structures. Structures which depend on cross-stream velocity fluctuations or are dependent on quantities that mix nominally large and small scales together, such as $\mathcal{R}$, $\mathcal{F}^{CS}_{\text{Turb.}}$, $\mathcal{F}_{\text{Press.}}$, $\mathcal{PS}^S$, and $\mathcal{PS}^{CS}$, have attached clusters which contribute between 60% and 75% of their total volume. Finally, structures which depend on gradients such as ϵ, $\mathcal{F}^S_{\text{Diff.}}$, and $\mathcal{F}^{CS}_{\text{Diff.}}$ have attached clusters which contribute between 50% and 56% of their total volume. The only exceptions within these gradient-based structures are vortex clusters, $\mathcal{D}$, which while being proportional to the sixth power of the velocity gradient tensor, have attached clusters which contribute 63% of their total volume. This is likely because these attached vortex clusters are indicators of strong $\mathcal{Q}$ events, as discussed by Del Álamo & Jiménez (2006).

By examining the average total volume occupied simultaneously by all different eddy types, $\overline{V}(\Omega_{\mathcal{Q}} \cup \Omega_{\mathcal{S}} \cdots \Omega_{\mathcal{PS}^S} \cup \Omega_{\mathcal{PS}^{CS}})$, we can determine whether a single eddy type is capable of highlighting all regions of intense activity in the flow. The answer appears to be negative, because even though no single eddy type occupies more than 18% of the flow domain, the average volume occupied by all eddy types simultaneously is $46 \pm 2\%$. If we only account for wall-attached clusters, $\overline{V}(\Omega^{\mathcal{A}}_{\mathcal{Q}} \cup \Omega^{\mathcal{A}}_{\mathcal{S}} \cdots \Omega^{\mathcal{A}}_{\mathcal{PS}^S} \cup \Omega^{\mathcal{A}}_{\mathcal{PS}^{CS}})$, then while no single eddy type occupies more than 15%, the average volume occupied by all eddy types is $36 \pm 3\%$. This indicates that while there might be a lot of overlap between different structure types, the regions which appear empty, given a single definition, might simply contain eddies which are representative of other dynamical processes, because $\max_{f_p} \overline{V}(\Omega_{f_p}) < \overline{V}(\Omega_{\mathcal{Q}} \cup \Omega_{\mathcal{S}} \cdots \Omega_{\mathcal{PS}^S} \cup \Omega_{\mathcal{PS}^{CS}}) < V_{\text{Domain}} < \Sigma_{f_p} \overline{V}(\Omega_{f_p})$. We now move on to quantifying this behavior in more detail.

3.2. *The relative volumetric intersection matrix*

To quantify how regions of space associated with different eddy types are contained within one another, we compute the average intersection volume of all two-set combinations of the presently analyzed 14 types of structures. This results in 91 possible intersections as the intersections are symmetric. Given the regions occupied by two different eddy types, Ω_A, and Ω_B, we compute the average intersection volume, $\overline{V}(\Omega_A \cap \Omega_B)$, between the two types and normalize $\overline{V}(\Omega_A \cap \Omega_B)$ independently by both $\overline{V}(\Omega_A)$ and $\overline{V}(\Omega_B)$ to quantify whether, on average, one eddy type is simply larger than the other and hence contains the other eddy type in its entirety. This would imply that detecting regions of the larger-on-average eddy type might suffice for capturing the dynamics of the other type given some postprocessing, but not necessarily vice versa. The results of this analysis for all

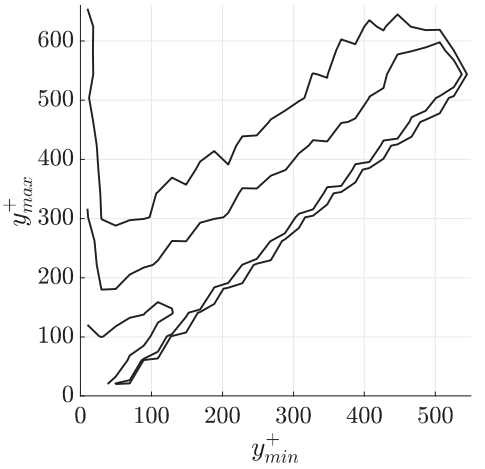

FIGURE 1. The joint PDF of the minimal and maximal wall-normal extents of the identified streaky eddies, $\mathcal{S}$. The contours are 0.1%, 0.5%, and 5% of the maximum value of the PDF.

detected structures, and only for those which are attached, are presented in Figures 2 and 3, respectively. The details of how to interpret the intersection matrices are in the caption of Figure 2.

A few key features become apparent when examining the two intersection matrices. First, $\mathcal{Q}$ structures, while strictly a wall-normal momentum-transfer structure, contain within them all $\mathcal{P}$ structures in their entirety and over 90% of the $\mathcal{F}^S_{\text{Turb.}}$ structures, as is evident by looking at the first columns of the two matrices. However, the opposite is not true; i.e., while there could be a strong energy transfer event, we could be missing a strong momentum-transfer event as they are larger in size. On the other hand, $\mathcal{P}$ and $\mathcal{F}^S_{\text{Turb.}}$ appear to be closer in size and relative overlap such that they could serve as surrogate signals for each other. Furthermore, streaky structures, $\mathcal{S}$, substantially overlap, and surprisingly equally, with both $\mathcal{Q}$ and $\mathcal{F}^S_{\text{Turb.}}$ regardless of the discrepancy between the overlap of $\mathcal{Q}$ and $\mathcal{F}^S_{\text{Turb.}}$ with each other. The cross-stream energy eddies, $\mathcal{R}$, overlap strongly, around two-thirds of the volume, with the $\mathcal{F}^{CS}_{\text{Turb.}}$ eddy type. The diffusive flux of streamwise energy eddies, $\mathcal{F}^S_{\text{Diff.}}$, weakly overlap with $\mathcal{Q}$, $\mathcal{P}$, and $\mathcal{F}^S_{\text{Turb.}}$ eddy types. On the other hand, diffusive cross-stream energy flux eddies, $\mathcal{F}^{CS}_{\text{Diff.}}$, do not seem to preferentially intersect with any other eddy type. This behavior is similar to that of the other small scale eddies such as ϵ and $\mathcal{D}$, although the intersection of $\mathcal{D}$ eddies with those which contain pressure is slightly higher than with other types. Finally, we consider pressure-type eddies. Overall, all pressure-type eddies, namely p, $\mathcal{F}_{\text{Press.}}$, $\mathcal{PS}^S$, and $\mathcal{PS}^{CS}$, except for a slightly weak intersection between $\mathcal{F}_{\text{Press.}}$ and $\mathcal{Q}$ and $\mathcal{P}$, seem to not intersect preferentially with any other non-pressure-type eddy. This finding could in fact be useful in defining interactions between eddies, as evasion can be considered a form of interaction, as discussed below.

3.3. *A plausible condition for "at-a-distance" spatiotemporal interactions between eddies*

Beyond the static analysis, a dynamic analysis would involve tracking each of the identified structures in time and space and constructing graphs which encode all merging, splitting, growth, and decay of individual structures (Lozano-Durán *et al.* 2014; Bae & Lee 2021; Elnahhas *et al.* 2024). These graphs are what we would refer to as spatiotem-

	$\mathcal{Q}$	$\mathcal{S}$	$\mathcal{R}$	p	$\mathcal{P}$	ϵ	$\mathcal{D}$	$\mathcal{F}^{\mathrm{S}}_{\mathrm{Turb.}}$	$\mathcal{F}^{\mathrm{CS}}_{\mathrm{Turb.}}$	$\mathcal{F}^{\mathrm{S}}_{\mathrm{Diff.}}$	$\mathcal{F}^{\mathrm{CS}}_{\mathrm{Diff.}}$	$\mathcal{F}_{\mathrm{Press.}}$	$\mathcal{PS}^{\mathrm{S}}$	$\mathcal{PS}^{\mathrm{CS}}$
$\mathcal{Q}$	1	0.27	0.19	0.19	0.87	0.08	0.11	0.71	0.28	0.22	0.17	0.34	0.17	0.17
$\mathcal{S}$	0.63	1	0.34	0.24	0.59	0.11	0.14	0.66	0.26	0.36	0.26	0.26	0.21	0.21
$\mathcal{R}$	0.46	0.36	1	0.26	0.43	0.13	0.17	0.34	0.67	0.16	0.44	0.41	0.25	0.25
p	0.23	0.13	0.13	1	0.2	0.11	0.2	0.18	0.13	0.14	0.17	0.5	0.52	0.51
$\mathcal{P}$	1	0.3	0.2	0.19	1	0.08	0.11	0.79	0.31	0.23	0.17	0.36	0.17	0.17
ϵ	0.29	0.17	0.2	0.31	0.26	1	0.44	0.22	0.2	0.32	0.4	0.29	0.45	0.45
$\mathcal{D}$	0.27	0.15	0.17	0.41	0.25	0.31	1	0.21	0.18	0.27	0.35	0.34	0.38	0.39
$\mathcal{F}^{\mathrm{S}}_{\mathrm{Turb.}}$	0.95	0.38	0.19	0.19	0.91	0.08	0.11	1	0.27	0.27	0.17	0.33	0.17	0.17
$\mathcal{F}^{\mathrm{CS}}_{\mathrm{Turb.}}$	0.64	0.26	0.64	0.25	0.61	0.13	0.17	0.47	1	0.16	0.36	0.54	0.24	0.24
$\mathcal{F}^{\mathrm{S}}_{\mathrm{Diff.}}$	0.51	0.37	0.16	0.27	0.47	0.21	0.25	0.48	0.16	1	0.21	0.25	0.27	0.27
$\mathcal{F}^{\mathrm{CS}}_{\mathrm{Diff.}}$	0.32	0.22	0.35	0.27	0.29	0.22	0.27	0.24	0.3	0.18	1	0.3	0.27	0.27
$\mathcal{F}_{\mathrm{Press.}}$	0.49	0.16	0.24	0.59	0.45	0.12	0.19	0.36	0.34	0.15	0.22	1	0.44	0.43
$\mathcal{PS}^{\mathrm{S}}$	0.23	0.13	0.14	0.59	0.21	0.17	0.21	0.18	0.15	0.16	0.19	0.43	1	0.86
$\mathcal{PS}^{\mathrm{CS}}$	0.24	0.13	0.15	0.6	0.21	0.18	0.22	0.18	0.15	0.17	0.2	0.43	0.88	1

FIGURE 2. The relative volumetric intersection matrix of all eddy types, accounting for all identified clusters. The diagonal saturates at one, as that is the volume of a single eddy type normalized by itself. The values in each row are normalized intersection volumes between types $\overline{V}(\Omega_A \cap \Omega_B)/\overline{V}(\Omega_A)$ where A is eddy type of the row and B is the eddy type of the column. The values in each column are the normalized intersection volumes between types $\overline{V}(\Omega_A \cap \Omega_B)/\overline{V}(\Omega_B)$ where A is eddy type of the column and B is the eddy type of the row.

poral eddies, or simply coherent structures in the sense of the definition introduced in Section 1. However, the original approach of Lozano-Durán *et al.* (2014), which only accounts for dynamical interactions between eddies through merging and splitting events, is agnostic to interactions which involve the flux of a quantity from one energy-carrying eddy to the next. These interactions, hidden from the standard single-type approach would be uncovered when multiple energy- and flux-carrying eddies are simultaneously tracked with both intra- and inter-type connections being tallied. Elnahhas *et al.* (2024) developed a general methodology to perform this multi-eddy-type tracking through the construction of multilayer networks (Boccaletti *et al.* 2014). However, their choices for the different types were limited, relying primarily on already well-defined types such as streaks, $\mathcal{S}$ (Bae & Lee 2021), and momentum-transfer structures, $\mathcal{Q}$ (Lozano-Durán *et al.* 2012, 2014; Elnahhas *et al.* 2022). Through the current intersection matrix analysis, we were able to verify that the space in between eddies of a single type is indeed occupied by eddies of other types. Hence, interactions between eddies of the same energy-carrying type involve not only spatial overlap, but also fluxes from one eddy to the next, through

	$\mathcal{Q}$	$\mathcal{S}$	$\mathcal{R}$	p	$\mathcal{P}$	ϵ	$\mathcal{D}$	$\mathcal{F}^{\mathrm{S}}_{\mathrm{Turb.}}$	$\mathcal{F}^{\mathrm{CS}}_{\mathrm{Turb.}}$	$\mathcal{F}^{\mathrm{S}}_{\mathrm{Diff.}}$	$\mathcal{F}^{\mathrm{CS}}_{\mathrm{Diff.}}$	$\mathcal{F}_{\mathrm{Press.}}$	$\mathcal{PS}^{\mathrm{S}}$	$\mathcal{PS}^{\mathrm{CS}}$
$\mathcal{Q}$	1	0.26	0.16	0.16	0.85	0.05	0.08	0.69	0.21	0.13	0.11	0.29	0.12	0.13
$\mathcal{S}$	0.62	1	0.28	0.21	0.57	0.07	0.11	0.64	0.2	0.26	0.19	0.23	0.16	0.17
$\mathcal{R}$	0.42	0.32	1	0.25	0.38	0.1	0.14	0.31	0.51	0.11	0.37	0.36	0.21	0.22
p	0.2	0.11	0.12	1	0.18	0.06	0.14	0.16	0.1	0.08	0.12	0.46	0.41	0.42
$\mathcal{P}$	1	0.29	0.17	0.17	1	0.05	0.09	0.78	0.23	0.15	0.12	0.3	0.12	0.13
ϵ	0.29	0.19	0.21	0.28	0.26	1	0.44	0.23	0.19	0.27	0.34	0.27	0.37	0.39
$\mathcal{D}$	0.27	0.16	0.18	0.36	0.24	0.24	1	0.22	0.17	0.17	0.29	0.33	0.32	0.34
$\mathcal{F}^{\mathrm{S}}_{\mathrm{Turb.}}$	0.92	0.37	0.16	0.17	0.88	0.05	0.09	1	0.2	0.18	0.11	0.28	0.12	0.13
$\mathcal{F}^{\mathrm{CS}}_{\mathrm{Turb.}}$	0.63	0.26	0.59	0.25	0.59	0.1	0.15	0.47	1	0.12	0.29	0.5	0.21	0.22
$\mathcal{F}^{\mathrm{S}}_{\mathrm{Diff.}}$	0.52	0.44	0.16	0.24	0.48	0.17	0.2	0.53	0.15	1	0.17	0.23	0.22	0.23
$\mathcal{F}^{\mathrm{CS}}_{\mathrm{Diff.}}$	0.31	0.23	0.39	0.28	0.27	0.16	0.24	0.23	0.26	0.12	1	0.29	0.23	0.25
$\mathcal{F}_{\mathrm{Press.}}$	0.45	0.15	0.22	0.58	0.4	0.07	0.16	0.32	0.26	0.09	0.17	1	0.36	0.37
$\mathcal{PS}^{\mathrm{S}}$	0.23	0.13	0.15	0.64	0.2	0.12	0.19	0.18	0.13	0.11	0.16	0.45	1	0.83
$\mathcal{PS}^{\mathrm{CS}}$	0.23	0.13	0.15	0.63	0.2	0.12	0.19	0.18	0.13	0.11	0.16	0.44	0.79	1

FIGURE 3. The relative volumetric intersection matrix of all eddy types, accounting for only the attached identified clusters. How to interpret this intersection matrix is described in the caption of Figure 2.

any of the flux terms $\mathcal{Q}$, p', $\mathcal{F}^{S}_{\mathrm{Turb.}}$, $\mathcal{F}_{\mathrm{Press.}}$, $\mathcal{F}^{CS}_{\mathrm{Turb.}}$, $\mathcal{F}^{S}_{\mathrm{Diff.}}$, and $\mathcal{F}^{CS}_{\mathrm{Diff.}}$, and inter-component redistribution terms $\mathcal{PS}^{S}$, and $\mathcal{PS}^{CS}$.

As such, a plausible condition for identifying an "at-a-distance" interaction between two eddies is the following:

Between every two interacting energy-carrying eddies, there exists a third eddy, of the flux-carrying type, which overlaps with both energy-carrying eddies to some degree.

Note that this condition for an "at-a-distance" interaction can occur even if there is no spatial overlap between the two constituent energy-carrying eddies themselves, as evasion could be considered a form of interaction, if facilitated by some flux from one eddy to the next. For example, from a momentum perspective, the collision of two eddies would be slowed down due to the increase in pressure between them. Given this perspective, we would be able to detect an interaction much earlier than if we were to wait for a spatial overlap to occur. An example is shown in Figure 4, where the slower, downstream

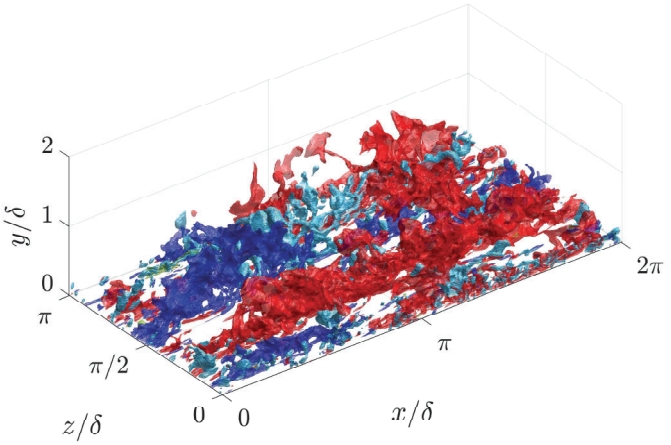

FIGURE 4. An example of an interaction between two eddies given an intermediate third one. Red eddies are strong ejection events. Dark blue eddies are strong sweep events. Cyan eddies are strong pressure events. Only eddies attached to the bottom wall are illustrated.

ejection is interacting with the faster, upstream sweep, due to the presence of a pressure fluctuation eddy between them.

4. Conclusions and future work

In this work, we sought answers to the following questions: Is there a single eddy definition which would highlight all regions of intense activity in a flow, leaving behind the unimportant regions? If not, what lies in the space in between regions of intense activity given a particular definition? We focused on only static quantities and computed the individual eddy type occupied volume, the total occupied volume by all eddies defined from the non-zero terms of the averaged Reynolds-stress budget equations, and the normalized volumes of intersection between all two-type sets of eddies. There is no single eddy definition which highlights all regions of space highlighted by all eddy-types simultaneously. This implies that in the empty space between regions considered important given some definition, another term, representative of another dynamical mechanism, is active. Therefore, we proposed that a condition for identifying "at-a-distance" interactions between any two energy (property)-carrying eddies that are not in spatial overlap is the presence of a third mediating eddy defined based on the flux of that energy (property) which itself touches the two eddies. This definition can of course be extended to a scale-dependent formalism, where eddies which carry energy at different scales are only considered to interact if an eddy, defined through the energy flux across scale terms, is present between them.

In the future, these eddies defined based on fluxes of energy across scale will be constructed using filtering approaches designed for inhomogeneous flows (Zhao & Aluie 2023) and applied to the network-motif analysis of turbulent coherent structures to identify the dynamical building blocks in both physical and scale space (Elnahhas *et al.* 2024).

Acknowledgments

A. Elnahhas acknowledges support from NASA grant #80NSSC20M0201. A. Elnahhas is also grateful for the fruitful discussions with T. Flint, E. Lenz, C. T. Williams, Prof. H. J. Bae, Prof. A. Lozano-Durán, Prof. N. T. Ouellette, and Prof. P. Moin.

REFERENCES

Adrian, R. J. 2007 Hairpin vortex organization in wall turbulence. *Phys. Fluids* **19**, 041301.

Bae, H. J. & Lee, M. 2021 Life cycle of streaks in the buffer layer of wall-bounded turbulence. *Phys. Rev. Fluids* **6**, 064603.

Boccaletti, S., Bianconi, G., Criado, R., del Genio, C. I., Gómez-Gardeñes, J., Romance, M., Sendiña-Nadal, I., Wang, Z. & Zanin, M. 2014 The structure and dynamics of multilayer networks. *Phys. Rep.* **544**, 1–122.

Del Álamo, J. C. & Jiménez, J. Self-similar vortex clusters in the turbulent logarithmic region. *J. Fluid Mech.* **561**, 329–358.

Dong, S., Huang, Y. Yuan, X. & Lozano-Durán, A. 2020 The coherent structure of the kinetic energy transfer in shear turbulence. *J. Fluid Mech.* **892**, A22.

Elnahhas, A., Lenz, E., Moin, P., Lozano-Durán, A. & Bae, H. J. 2024 Are the dynamics of wall turbulence in minimal channels and larger larger domain channels equivalent? A graph-theoretic approach. *J. Phys. Conf. Ser*. In press.

Elnahhas, A., Lozano-Durán, A. & Wallace, J. 2022 A geometrical comparison of the momentum-carrying structures between boundary layer transition and fully developed turbulence. *Proceedings of the Summer Program*, Center for Turbulence Research, Stanford University, pp. 323–333.

Frisch, U. 1995 *Turbulence: The Legacy of A. N. Kolmogorov.* Cambridge University Press.

Lozano-Durán, A., Flores, O. & Jiménez, J. 2012 The three-dimensional structure of momentum transfer in turbulent channels. *J. Fluid Mech.* **694**, 100–130.

Lozano-Durán, A. & Jiménez, J. 2014 Time-resolved evolution of coherent structures in turbulent channels: characterization of eddies and cascades. *J. Fluid Mech.* **759**, 432–471.

Lundgren, T. S. 1982 Strained spiral vortex model for turbulent fine structure. *Phys. Fluids* **25**, 2193–2203.

Mansour, N. N., Kim, J. & Moin, P. 1988 Reynolds-stress and dissipation-rate budgets in a turbulent channel flow. *J. Fluid Mech.* **194**, 15–44.

Marusic, I. & Monty, J. P. 2019 Attached eddy model of wall turbulence. *Annu. Rev. Fluid Mech.* **51**, 59–74.

Perry, A. E. & Chong, M. S. On the mechanism of wall turbulence. *J. Fluid Mech.* **119**, 172–217.

Robinson, S. K. 1991 Coherent motions in the turbulent boundary layer. *Annu. Rev. Fluid Mech.* **23**, 601–639.

Townsend, A. A. 1976 *The Structure of Turbulent Shear Flow.* Cambridge University Press. **2nd** edition

Zhao, D. & Aluie, H. 2023 Measuring scale-dependent shape anisotropy by coarse-graining; Application to inhomogeneous Rayleigh-Taylor turbulence. *Phys. Rev. Fluids* **8**, 114601.